
This is an electronic reprint of the original article.
This reprint may differ from the original in pagination and typographic detail.

Masyukov, Maxim; Vainshtein, Sergey; Grigorev, Roman; Taylor, Zachary

Fivefold Peak Power Boost in HBT-driven GaAs Collapsing-Field-Domain-Based Sub-THz Source

Published in:
IEEE Electron Device Letters

DOI:
[10.1109/LED.2023.3302015](https://doi.org/10.1109/LED.2023.3302015)

Published: 01/10/2023

Document Version
Peer-reviewed accepted author manuscript, also known as Final accepted manuscript or Post-print

Please cite the original version:
Masyukov, M., Vainshtein, S., Grigorev, R., & Taylor, Z. (2023). Fivefold Peak Power Boost in HBT-driven GaAs Collapsing-Field-Domain-Based Sub-THz Source. *IEEE Electron Device Letters*, 44(10), 1716-1719. Article 10208246. <https://doi.org/10.1109/LED.2023.3302015>

This material is protected by copyright and other intellectual property rights, and duplication or sale of all or part of any of the repository collections is not permitted, except that material may be duplicated by you for your research use or educational purposes in electronic or print form. You must obtain permission for any other use. Electronic or print copies may not be offered, whether for sale or otherwise to anyone who is not an authorised user.

Fivefold Peak Power Boost in HBT-driven GaAs Collapsing-Field-Domain-Based Sub-THz Source

Maxim Masyukov, *Student Member, IEEE*, Sergey Vainshtein, Roman Grigorev, and Zachary Taylor, *Member, IEEE*

Abstract—Miniature on-chip sources based on the collapsing field domain phenomenon in GaAs have advanced compact sub-picosecond time-domain imaging schemes operating in the 100-250 GHz frequency range. Efforts have been done to broaden the emission band of on-chip sources towards 400 GHz, but increasing the peak power of the emitted picosecond-range pulses remains physically challenging but practically important. In this work, a fivefold increase in peak power has been achieved by replacing the previously used hetero-bipolar-based collapsing field domain source operating in self-oscillating mode with a bipolar-based source externally pulsed by a hetero-bipolar driver. Importantly, the suggested solution unaffected the compactness of the source and facilitates its application in time domain imaging.

Index Terms—Terahertz waves, avalanche breakdown, solid-state terahertz (THz) pulsed source, submillimeter waves.

I. INTRODUCTION

Within the last few decades, time-domain spectroscopy (TDS) and time-domain imaging (TDI) have become accessible techniques via the implementation of femtosecond laser-driven pulsed sources [1]–[3]. Their recent applications include biophotonics [4], [5], security scanning [6], and other [7]. While the temporal resolution of such systems reaches hundreds of femtoseconds [8], [9], most TDI/TDS THz setups remain bulky, expensive, and energy-consuming, limiting their real-world applications.

Recent advances in the collapsing field domain (CFD) phenomenon in GaAs have led to the development of miniature, all-electronic on-chip sources for TDI with sub-picosecond temporal resolution [10], [11]. In such systems, a GaAs avalanche switch is integrated with a sub-mm-sized on-chip antenna, emitting a wavelet of ≤ 100 ps duration with a frequency band ranging from 100 to 250 GHz. Quasi-optical schemes have been used for both transmission and reflection TDIs. The band of the receiving channel (wave) at 20 GHz corresponds to the pulse front of (wave) 15 ps, and even a fraction of this front can provide a few ps of time-of-flight temporal resolution at best. This sub-picosecond TDI precision, demonstrated in Refs. [10], [11], was termed the

interferometric enhancement attributed to the interference of the wavelets in the reflection TDI scheme. This phenomenon makes the TDI temporal resolution in the CFD-based scheme comparable to bulky, costly, and complicated laser-driven TDI/TDS systems that require tuning.

To further advance CFD-source-based TDI, efforts are being made to broaden the emission band towards 400 GHz, which could lead to improved spatial resolution [12]. However, increasing the power of such sources could also open new applications. All CFD/TDI experiments presented so far use hetero-bipolar CFD (HBT-like, self-oscillating) emitter structures, and the peak power of those emitters did not exceed 0.2-0.3 mW [10], [11]. In the current work, we have achieved a fivefold enhancement by a proper electronic circuit design for driving the source. The results provide further usage of such sources in biophotonics, where the intensity of the THz waves plays a crucial role due to the strong water absorption [13].

II. DEVICE DESCRIPTION

HBT-like and BJT-like GaAs sources utilize the CFD phenomenon in the low-doped n^0 -collector of the transistor. The CFDs are formed in the avalanche-generated electron-hole (e-h) plasma due to negative differential mobility (NDM) at extreme electric fields [14]. The difference between CFD sub-THz sources and HBT/BJT transistors is in manipulating the n^0 - n^+ collector layers that allow control of the CFDs generation and annihilation [10], [12]. The electron injection efficiency from the emitter in HBT is significantly higher than in BJT due to the emitter hetero-barrier [15] for the holes, and a ledge [16] that prevents robust carrier recombination at the surface of the emitter-base junction. The BJT source, however, cannot switch actively. The HBT's efficient electron injection enables effective positive feedback between electron and hole injection. This results in rapid e-h plasma generation, CFD formation and collapse, and a subsequent decrease in collector voltage. As a result, high-current avalanche switching can occur quickly without any thermal impact on the structure, even with a slight increase in collector voltage beyond the avalanche breakdown threshold. The structure experiences initial avalanching at a high voltage, but rapid e-h plasma formation is crucial in preventing thermal breakdown. Consequently, slow and periodic growth in collector voltage across the HBT results in safe and periodic self-switching without posing any danger to the device. One should note that the length of the collector is an important parameter, and

This work was supported by Jane and Aatos Erkkö Foundation.

The authors are with the MilliLab, Department of Electronics and Nano-engineering, Aalto University, P.O. Box 15500, 00076 Aalto, Finland. Corresponding author: Maxim Masyukov (e-mail: maxim.masyukov@aalto.fi).

Dr. Sergey Vainshtein is also with the CAS group, Faculty of Information Technology and Electrical Engineering, the University of Oulu, FIN-90014 Oulu, Finland. Dr. Roman Grigorev is now with the Center for THz-driven Biological Systems, Department of Physics and Astronomy, Seoul National University, Seoul 151-747, South Korea

Manuscript received XX.XX.XXXX; revised XX.XX.XXXX.

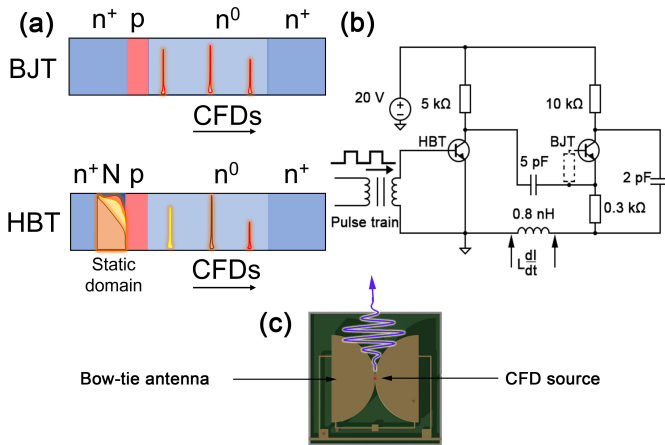


Fig. 1. (a) Schematic illustration of the electric field profiles in HBT and BJT. The interplay between moving (in n^0) and static (in N) domains, leading to partial compensation for the voltage change across the entire structure, is represented with brown, yellow, and red colored domains for each particular combination [10], [12]; (b) the electrical circuit with both the HBT driver and BJT CFD source; (c) a schematic representation of the on-chip CFD source (marked by the red dot) coupled to a bow-tie antenna emitting the sub-THz wavelet.

if the blocking voltage is not high enough, the current density required for THz generation cannot be achieved.

In contrast to HBT, in BJT, slow base-collector avalanche breakdown causes a high current at a large voltage, leading to thermal breakdown before self-switching. Preliminary tests show that passive CFD switching can work in BJT if the breakdown current saturates surface recombination, boosts injection efficiency, and enables usual CFD switching without thermal stress in the switching channel. However, this regime requires pulse generators that are, to the best of our knowledge, not commercially available and/or applicable in compact TDI schemes. Instead, we propose assembling a miniature Marx-type circuit with an HBT as the driving switch and a BJT as a source.

Passive switching is employed in BJT due to the significantly higher pulsed peak power typically observed from BJT-like emitters driven by an external pulse generator under comparable conditions (pulse duration, peak current amplitude across the device, and similar spectral properties). A quantitative difference in electric field profiles for HBT and BJT based on our previous simulations is shown in Fig. 1(a) [10], [12]. In both structures, the CFDs are formed in the n^0 layer near p -base, reach a quasi-steady-state amplitude (≈ 500 kV/cm) and width (≤ 100 nm), travel towards the n^+ -sub-collector with a velocity of 100 nm/ps, and then attenuate and collapse at its boundary. On average, two to three CFDs are observed simultaneously in the 700 nm n^0 layer. The main difference in the HBT's avalanche process is a large-amplitude static domain in the wide-band N -injector layer (see Fig. 1(a)). The static domain shape varies simultaneously with the formation and collapsing of moving CFDs, and the more prominent static domain corresponds to less intensive CFD. It partly compensates for the temporal (sub-THz) variation of the voltage across the structure, reduces the current across the antenna, and thus reduces the peak power emitted by the

HBT-based radiation source (see [10], [12] for the numerical simulations and more details about the operating mode)

The device under test' (DUT) circuit is shown in Fig. 1(b) operates as follows. The capacitors of 5 pF and 2 pF are charged to 20 V each one between the pulses across the resistors of 5 and 10 kOhm, respectively. The transformer's secondary winding shortens the emitter and base of the HBT, which ensures its highest possible breakdown voltage. The pulse from a generator is applied to the transformer, which triggers the avalanche switching of HBT and produces a negative voltage ramp. This ramp is then applied to the emitter of BJT, resulting in its avalanche switching. When almost a doubled breakdown voltage is applied to BJT, it leads to intense impact ionization in the picosecond-range, formation of an avalanching channel with e-h plasma, CFD generation, and picosecond-range avalanche switching of BJT. This process feeds the bow-tie antenna sub-THz current oscillations, and a 100 ps wavelet of 100-200 GHz is emitted (Fig. 1(c)). The voltage pulses $L \frac{dI}{dt}$ across $L=0.8$ nH inductance enable the triggering of an electrical oscilloscope, as shown in Fig. 2, which is synchronized with free-space-emitted sub-THz pulses. The procedure of the circuit parameters and antenna optimization is based on several goals, such as minimizing the parasitic inductance, as well as tuning the capacitors until the shortest possible pulse response with the highest peak power estimate is achieved.

In our study, we use just a single BJT as an emitter. Several BJTs may also have a chance to operate in a similar circuit, however, it increases the parasitic inductance of the circuit loop, which is a very sensitive parameter for such a transmitter in focus. In principle, such BJT emitter can be also fed by a circuit employing a GaN field-effect transistor (FET), but even the GaAs HBT-based solution operating in an avalanche mode has significant advantages with respect to the GaN FET-based solution. These advantages include the chip configuration and size considerations, allowing minimal possible inductance of the circuit loop to be achieved; switching speed, which is well below 100 ps; as well as the triggering simplicity, avoiding complicated requirements for the triggering circuit.

III. RESULTS AND CONCLUSIONS

A miniature double-side PCB with the device under test incorporating both HBT and BJT chips is placed in front of an elliptic mirror. The whole DUT is driven by a 5 V, 50 ns pulse across 50 Ω with a rise time of 5 ns. The BJT chip is positioned in the first focus of the mirror. The wavelet, emitted by the source, is collected by a zero-bias Schottky diode detector (Virginia Diodes), placed in the second focus of the mirror. The detector response is then amplified using a 0.1-26 GHz/30 dB MITEQ Microwave Amplifier and recorded with an oscilloscope triggered by the $L \frac{dI}{dt}$ electrical pulse. The optical system has been preliminary aligned, and then the detector position was fine-tuned with a precise 3D positioning system to achieve the maximal amplitude of the pulse. A set of band-pass filters with a full width at half maximum (FWHM) band of approximately 25 % of the central frequency was utilized to characterize the spectrum of the emitted electromagnetic signal. The quantitative estimation of the peak power

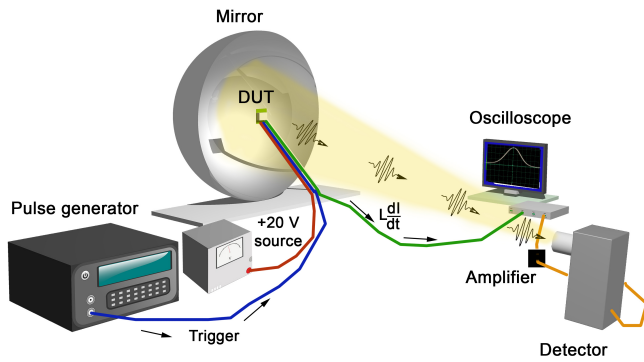


Fig. 2. The experimental setup for the DUT measurements: a pulse generator triggers the HBT avalanche switch, and the negative ps-range voltage ramp drives BJT being applied to its emitter. The BJT-coupled bow-tie antenna is placed at the first focal point of the elliptic mirror. Then, we use the voltage pulse $L \frac{dI}{dt}$ across the inductance for the oscilloscope triggering and simultaneously numerically evaluate the current pulse's shape and amplitude across BJT. The detector (either the Schottky diode or the Goly cell) is placed in the second focus of the mirror.

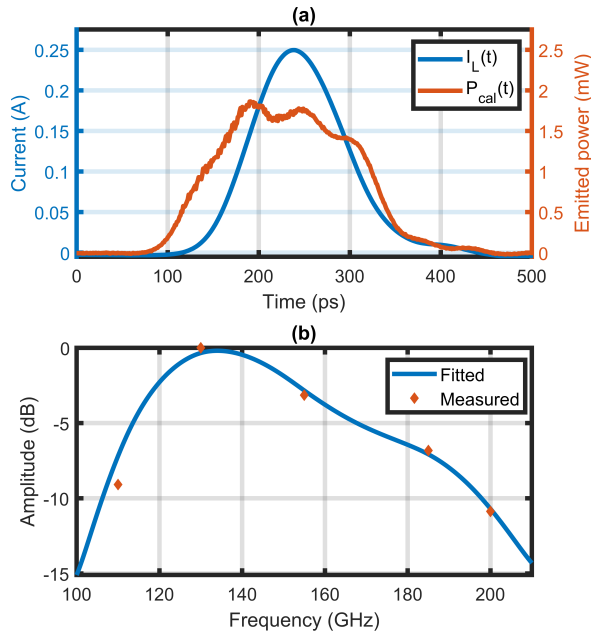


Fig. 3. (a) The current $I_L(t)$ across the BJT numerically computed from the measured $L \frac{dI}{dt}$ waveform, the sub-THz pulse power P_{cal} normalized by the experimentally estimated peak power using Goly cell. (b) The estimated spectrum of the emitted pulse obtained using the band-pass filter set.

was performed using the Goly cell, which has a verified responsivity of $6 \cdot 10^4$ V/W for a 15 Hz meander. Specifically, a burst of 100 ps sub-THz pulses, repeated at a rate of 1 MHz and lasting for 67 ms, was collected by the Goly cell sensor using the elliptic mirror, followed by a signal gap lasting 67 ms. The amplitude of the meander in the Goly cell output provided the average power within a burst, while the peak power in a 100 ps pulse was obtained by multiplying the average power by roughly $(100(ps) \cdot 1(MHz))^{-1}$ duty cycle.

The key takeaway from the measurement results (Fig. 3) is that the peak power output of calibrated power $P_{cal} \approx 1.7$ mW

is at least five times higher than the maximum peak power of 0.3 mW achieved from the self-oscillating, HBT-based CFD source, previously demonstrated in TDI applications [10], [11]. The current across BJT and the sub-THz emission is illustrated in Fig. 3 (a), where the current increase reflects the growing density of the conductive e-h plasma, which CFDs mainly form and then cause sub-THz current oscillations in the bow-tie antenna. Meanwhile, the generation of electrons and holes also increases; consequently, the emission reaches its peak earlier than the current. During the entire current pulse, the voltage across the structure decreases monotonically as the CFDs shrink and then collapse. This implies that the domains completely disappear when the sub-THz emission ceases at the time instant of ≈ 350 ps in Fig. 3(a), and the voltage across the structure also reaches a minimum. During the switching, we expect the current density in the avalanching channels to be around $10 MA/cm^2$, with a channel area of approx. $2 \mu m^2$. A stable sub-THz pulse corresponds to the switching event involving only one filament. The spectrum obtained from the measurement (Fig. 3(b)) exhibits a peak at 130 GHz, which corresponds to the time taken by the domain to traverse a 700 nm n^0 layer with a velocity of 100 nm/ps, consistent with previous simulations. To estimate the spectrum of the source, a set of bandpass filters (3-dB bandwidth $BW_{3dB} \approx 0.15 f_r$ at the resonant frequency f_r) fabricated according to the Ref. [17] have been utilized. The bandwidth of the spectrum peak, with an FWHM of approximately 35 GHz, is similar to the FWHM of the band-pass filters utilized. Therefore, it cannot be concluded that this value characterizes the behavior of only CFDs.

Summarizing, we have demonstrated a factor of five growth in the peak power generated by BJT-type CFD-based source compared to that of HBT-type. The price for this enhancement consists of the requirement of an external driving of BJT, unlike the user-friendly self-oscillating mode used in HBT. Also, it should be highlighted, that it is possible to use HBT for both source and a driver, in general, however, preliminary experiments demonstrated lower emitted power, as well as a complicated shape of the pulses [18]. Nevertheless, we suggested a miniature and cost-effective solution for the high-speed driver, which makes a practical application of BJT-type source realistic.

REFERENCES

- [1] J. A. Fülöp, S. Tzortzakis, and T. Kampfrath, "Laser-driven strong-field terahertz sources," *Advanced Optical Materials*, vol. 8, no. 3, p. 1900681, 2020, doi: 10.1002/adom.201900681.
- [2] A. Leitenstorfer, A. S. Moskalenko, T. Kampfrath, J. Kono, E. Castro-Camus, K. Peng, N. Qureshi, D. Turchinovich, K. Tanaka, A. Markelz *et al.*, "The 2023 terahertz science and technology roadmap," *Journal of Physics D: Applied Physics*, 2023, doi: 10.1088/1361-6463/acbe4c.
- [3] M. Tonouchi, "Cutting-edge terahertz technology," *Nature photonics*, vol. 1, no. 2, pp. 97–105, 2007, doi: 10.1038/nphoton.2007.3.
- [4] P. Bawuah and J. A. Zeitler, "Advances in terahertz time-domain spectroscopy of pharmaceutical solids: A review," *TrAC Trends in Analytical Chemistry*, vol. 139, p. 116272, 2021, doi: 10.1016/j.trac.2021.116272.
- [5] K. I. Zaytsev, V. N. Kurlov, M. Skorobogatiy, I. V. Reshetov, and V. V. Tuchin, "Special section guest editorial: advances in terahertz biomedical science and applications," *Journal of Biomedical Optics*, vol. 26, no. 4, pp. 043 001–043 001, 2021, doi: 10.1117/1.JBO.26.4.043001.

- [6] S. Mansourzadeh, D. Damyanov, T. Vogel, F. Wulf, R. B. Kohlhaas, B. Globisch, T. Schultze, M. Hoffmann, J. C. Balzer, and C. J. Saraceno, "High-power lensless thz imaging of hidden objects," *IEEE Access*, vol. 9, pp. 6268–6276, 2021, doi: 10.1109/ACCESS.2020.3048781.
- [7] G. Valušis, A. LISAUSKAS, H. Yuan, W. Knap, and H. G. Roskos, "Roadmap of terahertz imaging 2021," *Sensors*, vol. 21, no. 12, p. 4092, 2021, doi: 10.3390/s21124092.
- [8] A. Bartels, R. Cerna, C. Kistner, A. Thoma, F. Hudert, C. Janke, and T. Dekorsy, "Ultrafast time-domain spectroscopy based on high-speed asynchronous optical sampling," *Review of Scientific Instruments*, vol. 78, no. 3, p. 035107, 2007, doi: 10.1063/1.2714048.
- [9] P. Han and X. Zhang, "Free-space coherent broadband terahertz time-domain spectroscopy," *Measurement Science and Technology*, vol. 12, no. 11, p. 1747, 2001, doi: 10.1088/0957-0233/12/11/301.
- [10] S. N. Vainshtein, G. Duan, V. A. Mikhnev, V. E. Zemlyakov, V. I. Egorin, N. A. Kalyuzhnyy, N. A. Maleev, J. Näpänkangas, R. B. Sequeiros, and J. T. Kostamovaara, "Interferometrically enhanced sub-terahertz picosecond imaging utilizing a miniature collapsing-field-domain source," *Applied Physics Letters*, vol. 112, no. 19, p. 191104, 2018, doi: 10.1063/1.5022453.
- [11] V. A. Mikhnev, S. N. Vainshtein, and J. T. Kostamovaara, "Time-domain terahertz imaging of layered dielectric structures with interferometry-enhanced sensitivity," *IEEE Transactions on Terahertz Science and Technology*, vol. 10, no. 5, pp. 531–539, 2020, doi: 10.1109/TTHZ.2020.3003500.
- [12] S. N. Vainshtein, G. Duan, V. S. Yuferev, V. E. Zemlyakov, V. I. Egorin, N. A. Kalyuzhnyy, N. A. Maleev, A. Y. Egorov, and J. T. Kostamovaara, "Collapsing-field-domain-based 200 ghz solid-state source," *Applied Physics Letters*, vol. 115, no. 12, p. 123501, 2019, doi: 10.1063/1.5091616.
- [13] Q. Sun, R. I. Stantchev, J. Wang, E. P. Parrott, A. Cottenden, T.-W. Chiu, A. T. Ahuja, and E. Pickwell-MacPherson, "In vivo estimation of water diffusivity in occluded human skin using terahertz reflection spectroscopy," *Journal of biophotonics*, vol. 12, no. 2, p. e201800145, 2019, doi: 10.1002/jbio.201800145.
- [14] S. Vainshtein, V. Yuferev, and J. Kostamovaara, "Ultrahigh field multiple gunn domains as the physical reason for superfast (picosecond range) switching of a bipolar gaas transistor," *Journal of applied physics*, vol. 97, no. 2, p. 024502, 2005, doi: 10.1063/1.1839638.
- [15] N. L. Wang, W. J. Ho, and J. Higgins, "Algaas/gaas hbt linearity characteristics," *IEEE Transactions on Microwave Theory and Techniques*, vol. 42, no. 10, pp. 1845–1850, 1994, doi: 10.1109/22.320763.
- [16] Y. Chou and R. Ferro, "V. heterojunction bipolar transistors," *GaAs MMIC Reliability Assurance Guideline forSpace Applications*, p. 44, 1996.
- [17] D. W. Porterfield, J. Hesler, R. Densing, E. Mueller, T. Crowe, and R. Weikle, "Resonant metal-mesh bandpass filters for the far infrared," *Applied Optics*, vol. 33, no. 25, pp. 6046–6052, 1994, doi: 10.1364/AO.33.006046.
- [18] M. S. Masyukov, S. N. Vainshtein, J. Mallat, and Z. Taylor, "Contactless terahertz sensing of ultrafast switching in marx generator based on avalanche transistors," *IEEE Electron Device Letters*, vol. 43, no. 10, pp. 1724–1727, 2022, doi: 10.1109/LED.2022.3199996.